An experimental investigation of two active segmented partition arrays

Timothy W. Leishman[a)]
Acoustics Research Group, Department of Physics and Astronomy, Brigham Young University, Eyring Science Center, Provo, Utah 84602

Jiri Tichy
Graduate Program in Acoustics, The Pennsylvania State University, Applied Science Building, University Park, Pennsylvania 16802

(Received 20 December 2004; revised 27 July 2005; accepted 3 August 2005)

This paper addresses the construction, measurement, and analysis of two active segmented partition arrays (ASP arrays) for use in active sound transmission control. The control objective for each array was to actively minimize principal transmitting surface vibrations to induce high transmission loss. The arrays incorporated four adjacent lightweight modules with composite single or double leaves and small loudspeakers as actuators. A normal-incidence transmission loss measurement system was developed to evaluate their performances under passive and active conditions. Measurement results were compared to results for passive benchmark partitions and theoretical predictions. Four decentralized single-error-input, single-output filtered-x controllers were used with the arrays. They were shown to perform at least as well as a centralized multiple-error-input, multiple-output controller, with good error signal reductions and stability. Scanning laser vibrometer measurements confirmed the ability of the double-composite-leaf ASP to efficiently and globally minimize its transmitting surface vibrations to produce high transmission loss. Its average transmission loss over the active measurement bandwidth (30–290 Hz) was 56 dB—a full 34 dB greater than that of the single-composite-leaf ASP. The work confirms that a properly configured lightweight ASP can produce very high transmission loss through vibration control techniques. [DOI: 10.1121/1.2047348]

PACS number(s): 43.40.Vn, 43.50.Ki, 43.55.Rg [KAC] Pages: 3050–3063

I. INTRODUCTION

An active segmented partition (ASP) is a contiguous array of interconnected modules or elements that are specifically configured and controlled to reduce sound transmission between a source space and a receiving space. Several authors have investigated ASPs in recent years for distinct purposes.[1–9] The authors of this paper have explored them with the general aim of controlling sound transmission through lightweight structures via efficient, global control of transmitting surface vibrations.[10–17] One recent investigation[16] explored background and basic concepts of ASP design and use, focusing on modeling, theoretical analysis, and numerical transmission loss predictions for four individual module configurations. Two modules involved single-composite-leaf (SCL) configurations and two involved double-composite-leaf (DCL) configurations. Each was considered a candidate to fulfill one or more design and performance criteria established earlier.[10] Analytical and numerical results predicted that the two DCL arrangements would provide much greater transmission loss than the two SCL arrangements. However, only one of the DCL configurations (configuration 4 of Ref. 16) incorporated specialized segmentation and isolation to reduce coupling between adjacent partition modules. These characteristics were expected to enhance the effectiveness of the configurations in extended arrays using simple decentralized controllers.

A recent experimental study[17] validated the modeling and theoretical predictions for two individual modules from Ref. 16: configuration 2 (a SCL arrangement) and configuration 3 (a DCL arrangement). Experimental testing of configuration 1 (a SCL arrangement) and configuration 4 (a DCL arrangement), and evaluations of *arrays* of modules then became primary focuses of the present work. Because arrays of modules more closely represent practical ASPs, their distinguishing characteristics must be carefully considered.

Two experimental ASP arrays were designed and constructed for this investigation. Both consisted of four adjacent lightweight modules in square patterns. A normal-incidence transmission loss measurement system was also built for their evaluation. The properties of the arrays were determined under passive and active conditions and compared to theoretical predictions and properties of passive benchmark partitions. Scanning laser vibrometer measurements demonstrated the ability of the DCL arrangement to efficiently and globally minimize its transmitting surface vibrations.

The investigation also compared the normal-incidence transmission loss performance of the DCL ASP with that of the SCL ASP. It explored behaviors of decentralized (decoupled) and centralized (coupled) adaptive controllers in con-

a)Electronic mail: tim_leishman@byu.edu

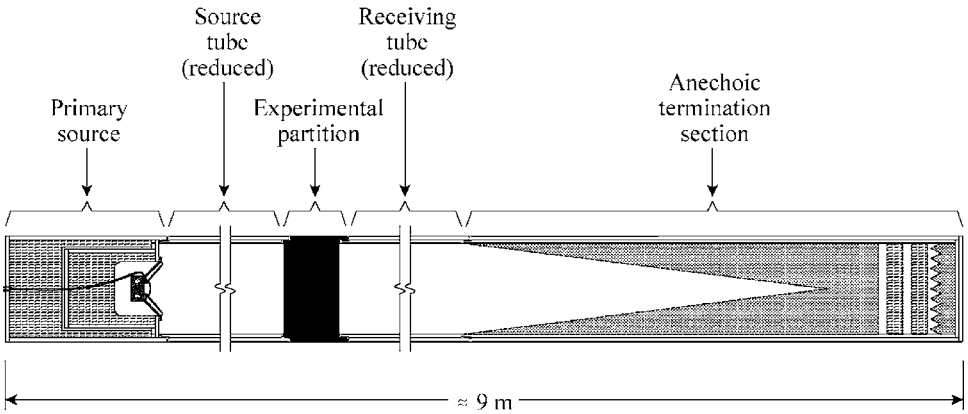

FIG. 1. A system for measuring normal-incidence transmission losses of test partitions (shown with an arbitrary partition positioned between the source tube and receiving tube).

junction with the arrays.[18] While the experimental arrays primarily used multiple single-error-input, single-output (multiple SISO or MSISO) filtered-x controllers, the DCL ASP also used a centralized multiple-error-input, multiple-output (MIMO) filtered-x controller for comparison.

The following sections discuss the apparatuses, techniques, and challenges associated with the evaluations. They also present key experimental results, draw pertinent conclusions, and provide recommendations for further research.

II. EXPERIMENTAL METHODS

The experimental methods used in this work were generally similar to those described in Ref. 17. However, many of the specific measurement apparatuses and capabilities were different. The transducers and electronics also varied in types and numbers. The following sections outline several details of the experimental approach.[19]

A. Normal-incidence measurement system

The normal-incidence measurement system is depicted in Fig. 1, with an arbitrary partition (ASP array or passive benchmark partition) positioned between the source and receiving tubes. The square tubes were basically identical in construction, with 47.6 cm $\times$ 47.6 cm interior cross-sectional dimensions and 244 cm nominal lengths. Their walls were constructed of two laminated layers of 1.9-cm-thick medium density fiberboard (MDF).

The primary source shown to the left of the source tube was an NHT 1259 loudspeaker (25.4 cm effective radiating diameter) that was front mounted on a double-walled sealed enclosure. All sections of the measurement system were constructed with undersized male and oversized female ends for convenient interconnection and isolation. Thick resilient double gaskets and adjustable clamps produced required air-tight seals. The overall length of the entire plane-wave tube system was approximately 9 m, although its exact length depended upon the particular partition under evaluation.

To limit the fields incident upon partitions to normally propagating plane waves, the source tube was consistently driven below the cutoff frequency of its first cross mode (approximately 360 Hz). At sufficient axial distances from the primary source and partition, the total upstream and downstream fields were accordingly dominated by plane waves. However, because residual effects of the first cross mode[20] or corruption due to vibrating tube walls became conspicuous in the measured field above 290 Hz, this latter frequency was considered the maximum plane-wave frequency of interest.

Most experimental partitions measured in the system produced boundary conditions that yielded significant axial source tube resonances. To address resulting measurement problems, the source loudspeaker was driven more vigorously at some frequencies (i.e., near tube antiresonance frequencies) than at others (i.e., near tube resonance frequencies). Because of its inconsistent vibration amplitude, structure-borne or air-borne flanking transmission often became more conspicuous near the source tube *antiresonance* frequencies. The tube walls were significant paths in flanking transmission at these and other frequencies.

As shown in Fig. 1, the receiving tube was bounded by a large anechoic termination. It was an inverted pyramidal structure cut from blocks of 25.6 kg/m^3 open-cell polyurethane foam rubber. When assembled, it tapered from a 47.6 cm $\times$ 47.6 cm opening to a central point over a 180.3 cm span. The base behind the point was a 25.4-cm-thick continuous extension of the wedge pieces, backed by a 38.1-cm-thick air cavity filled with layers of fiberglass insulation and open-cell polyurethane foam rubber. The cavity was capped with a rigid plug consisting of two laminated layers of 1.9-cm-thick MDF. The overall absorptive length of the termination was approximately 244 cm. Its measured cutoff frequency was about 45 Hz, but its absorption coefficient exceeded 0.7 down to nearly 10 Hz.[21]

B. ASP arrays

As indicated earlier, the first experimental ASP array consisted of a cluster of four adjacent SCL modules in a square pattern. The second consisted of a similar pattern of DCL modules. Both used Aura AS4-75-8 FR moving-coil loudspeakers as actuators. The drivers were designed with radially oriented neodymium magnet structures that permitted compact size, relatively low total mass (214 g), and reasonable low-frequency output. Their diaphragm dust domes were coated with several layers of epoxy to provide sufficiently rigid surfaces for accelerometer mounting. The following sections consider the design and construction of the two arrays in greater detail.

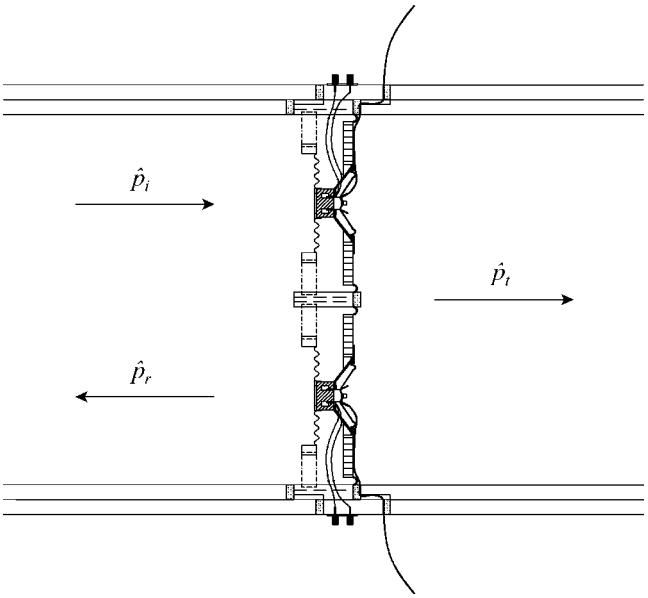

FIG. 2. A cutaway side view of the SCL ASP array. The view exposes two of the four adjacent modules with accelerometers mounted to the actuator dust domes. The array is connected to the source and receiving tubes via resilient airtight gaskets.

1. Single-composite-leaf (SCL) array

Figure 2 illustrates the SCL array in a cutaway side view that exposes two of the four modules. It also shows the interconnection of the array to the source and receiving tubes. Photographs of the array, taken from both the source side and transmitting side, are shown in Fig. 3. The actuators were mounted and sealed within centered 9.3-cm-diam openings of square resiliently suspended support panels. The panels were lightweight aluminum honeycomb sandwich constructions with dimensions of $20.9\ \text{cm} \times 20.9\ \text{cm} \times 1.6\ \text{cm}$ $(H \times W \times D)$ and average net masses of 87 g. They were stiffness controlled over the bandwidth of interest, exhibiting an average fundamental bending mode resonance frequency of about 940 Hz with no surround or actuator attached (i.e., with free boundary conditions). When these elements were attached, the frequency dropped slightly to approximately 865 Hz.

The panels were centered and resiliently attached within $22.9\ \text{cm} \times 22.9\ \text{cm}$ openings of an MDF frame using square half-roll compressed foam-rubber surrounds. They effectively behaved as large finite impedance interstices.[16] The 1.9-cm-thick MDF frame elements might also be termed interstices, but their large stiffnesses and small cross-sectional areas were expected to have very little effect on sound transmission.

The rear portions of the actuator magnet structures were firmly attached to perforated circular disks that were suspended from perforated support structures with porous secondary suspensions (spiders). These suspensions and the accompanying supports were intended to be acoustically unobtrusive over the frequency range of interest. The primary function of the spiders was to operate in conjunction with the support panel surrounds to produce spaced dual suspensions that helped constrain translational rigid-body motion of the support panels.

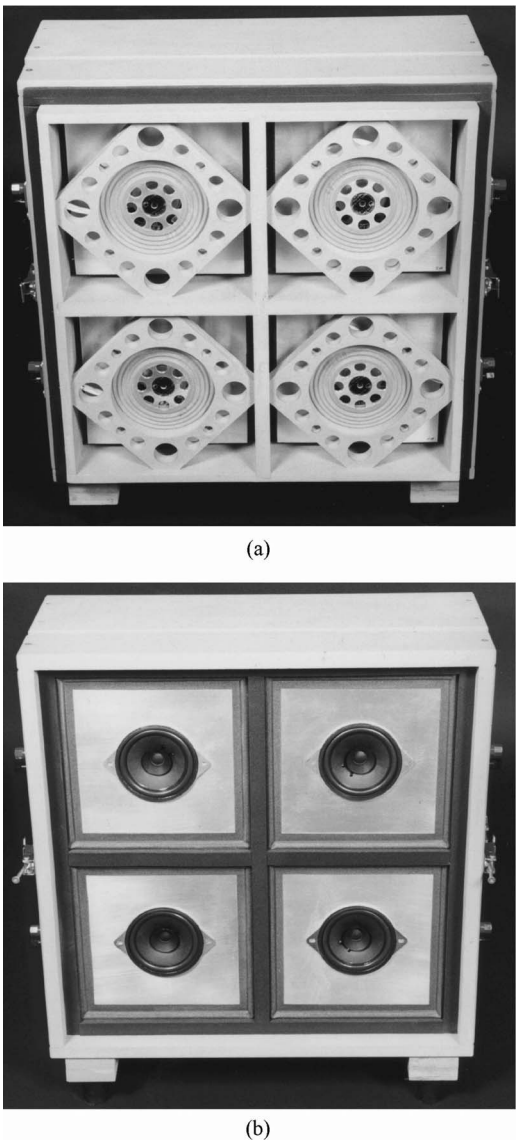

FIG. 3. Photographs of the experimental SCL array. (a) Source side. (b) Transmitting side.

As a rule-of-thumb, half of the flexing surface areas and masses of the suspensions were added to the surface areas and masses of the support panels for numerical predictions of array behaviors. The other halves were added to the presumably rigid MDF interstices. The net masses of the actuators (their total masses minus the moving masses of their diaphragm assemblies), the masses of the perforated secondary suspension mounting disks, and the masses of various adhesives were also added to the masses of the support panels to yield an average moving mass of approximately 340 g. This mass and the actuator diaphragm mass could vary slightly, depending upon accelerometer mounting and other conditions.

The array was intended to be tested in both its passive and active modes. The passive mode involved open-circuited actuator terminals, whereas the active mode involved the minimization of all normal actuator diaphragm accelerations.

2. Double-composite-leaf (DCL) array

Figure 4 shows a cutaway side view of the DCL array. Once again, each module of the array included a circular

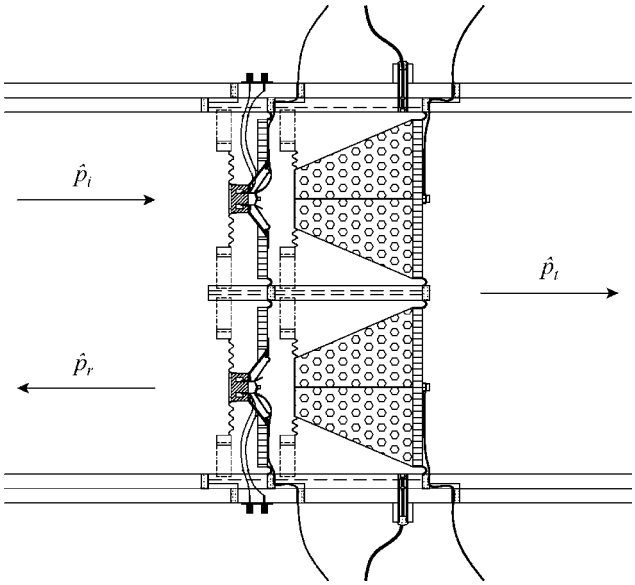

FIG. 4. A cutaway side view of the DCL ASP array. The view exposes two of the four adjacent modules with accelerometers mounted to the actuator dust domes and passive transmitting diaphragms. Cavity microphones are positioned behind the transmitting diaphragm surrounds. The actuator and transmitting diaphragm assemblies are joined by a resilient airtight connection.

moving-coil actuator surrounded by a square resiliently suspended support panel. In fact, the SCL array was an integral part of the DCL array. The photograph in Fig. 5 shows the actuator section being joined to the transmitting diaphragm section. In this arrangement, the actuators drove isolated rectangular cavities with passive transmitting diaphragms on the opposite sides.

The transmitting diaphragms were lightweight aluminum honeycomb sandwich panels similar in fabrication to the actuator support panels. They were centered and resiliently attached within 22.9 cm $\times$ 22.9 cm openings using similar half-roll compressed foam rubber surrounds. Perforated 0.8-mm-thick aluminum fins were attached in a crossing pattern to the back faces of the panels. They extended perpendicularly from the panels to thin perforated circular aluminum plates, which in turn were connected to spaced secondary suspensions (spiders). The fins were mounted to the panels along the crossing nodal lines of their first bending modes to help reduce mechanical excitation of those modes. The spiders were similar to those used in the SCL array and were again intended to help constrain translational piston-like motion of the transmitting diaphragms. Photographs of the transmitting diaphragm sections, taken from both the cavity and transmitting sides, are shown in Fig. 6.

FIG. 5. A photograph of the experimental DCL array, being formed by joining the SCL actuator array to the passive transmitting diaphragm array.

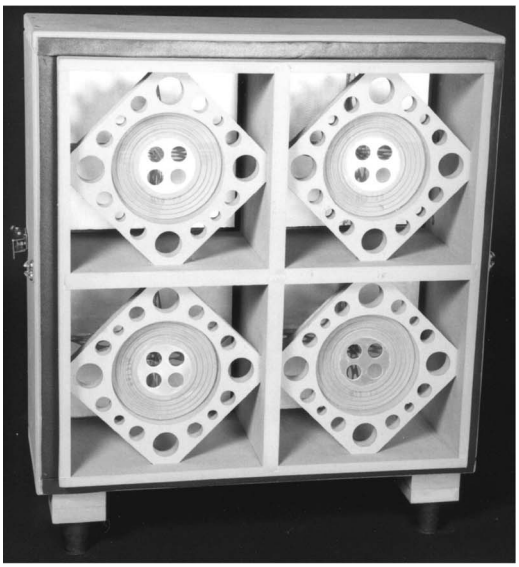

(a)

(b)

FIG. 6. Photographs of the transmitting diaphragm array portion of the experimental DCL array. (a) Cavity side. (b) Transmitting side.

The transmitting diaphragms were stiffness-controlled over the bandwidth of interest, exhibiting an average fundamental bending mode frequency of approximately 1020 Hz with all elements attached. Accounting for the masses of the fin structures, one half the masses of the suspensions, and the masses of adhesives, the average total moving mass of a transmitting diaphragm assembly was approximately 185 g. This mass could also vary slightly, depending upon accelerometer mounting and other conditions.

The DCL array was intended to be tested in both its passive mode (actuator terminals open-circuited) and in its active mode (normal transmitting diaphragm accelerations

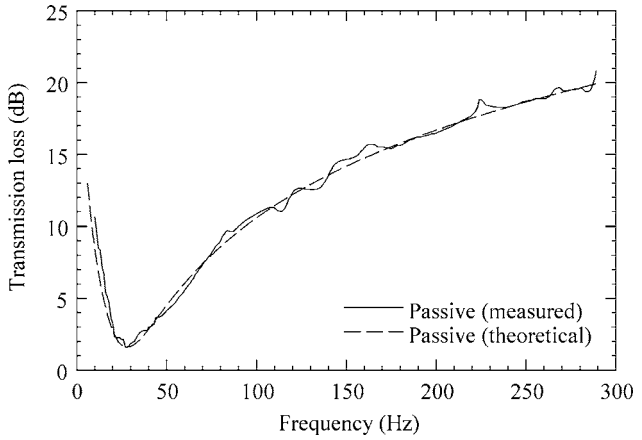

FIG. 7. The measured transmission loss for the passive transmitting diaphragm array. The measured curve is plotted against a theoretical prediction.

minimized). Acoustic pressures at positions within the module cavities could also be directly minimized through active control. However, the results produced by this scheme were very similar at low frequencies to those produced by the acceleration control scheme. This paper reports only the latter.

C. Passive benchmark partitions

Several passive benchmark partitions were developed to validate the performances of both the measurement system and the ASP arrays. Five structures were used for this purpose: (1) an open tube (no partition in place), (2) a lightweight single-leaf partition segmented into four modules, (3) a massive single-leaf partition filled with concrete, (4) a massive single-leaf partition filled with sand, and (5) a massive double-leaf partition consisting of both the concrete-filled and sand-filled leaves with various leaf spacings.

The measured transmission loss of the first benchmark "partition" (open tube) had an average value[22] of less than 0.3 dB over the passive measurement bandwidth (20–290 Hz). It gradually rose from very small values ($\approx$0 dB) at lower frequencies to around 2 dB at higher frequencies. The simple arrangement was tested to verify the ability of the system to measure very small transmission losses and to quantify system losses.

The second benchmark partition (segmented single-leaf partition) was the isolated passive transmitting diaphragm section of the DCL ASP array (see Fig. 6). The measured transmission loss for the partition is shown in Fig. 7, along with a theoretical prediction. The theoretical curve is based on modeling results from Refs. 13 and 16, the average moving diaphragm mass of the modules, the effective suspension compliance (derived from the mass and the 28 Hz resonance frequency), and an effective suspension resistance (derived from the transmission loss at resonance).[23] As suggested earlier, it assumes that the effective transmitting surface areas of the modules incorporate the inner flexing halves of their surrounds. The outer halves are treated as though they formed portions of the presumably rigid surrounding interstices.

The third benchmark partition was constructed using spaced MDF panels that spanned the partition cross section to form a 15.2-cm-thick cavity that was filled solid with concrete. The overall partition mass was approximately 85 kg. The fourth benchmark partition was similar to the concrete-filled partition, but it had a 10.2-cm-thick cavity filled with dry sand. Its overall mass was approximately 40 kg. The fifth benchmark partition provided the highest passive transmission loss. It consisted of a double-leaf structure involving both the concrete-filled and sand-filled leaves, with varying spacings and interconnections. The spacings included (1) a minimal separation of approximately 1 cm (provided only by compressed resilient gaskets), (2) a moderate separation of approximately 17 cm (provided by a spacer and resilient gaskets), and (3) a wide separation of approximately 175 cm with no direct structural connection. For the first two spacings, the adjustable gasket compression clamps could be configured with or without resilient rubber pads between their sections.

As detailed in Ref. 13, these massive benchmark partitions produced transmission loss curves that followed theoretical predictions to an extent. They also revealed measurement system limitations. Analyses showed that the system was capable of measuring partition transmission losses up to about 60 dB—except between 155 and 190 Hz, and above 225 Hz. In these isolated regions, flanking transmission reduced the reliability of measured values greater than about 45 dB. Interesting transmission loss anomalies were consistently found in regions near 175 and 245 Hz, both of which were axial antiresonance frequencies of the source tube. Measurements of partitions with very high transmission loss could produce higher values (at some frequencies) than those indicated. However, because much higher values could have been corrupted (e.g., from downstream interference produced by multiple transmission paths), they were generally considered with a degree of uncertainty.

D. Transducers

Small Kistler and PCB Piezotronics accelerometers were used to measure normal accelerations of several vibrating surfaces: actuator diaphragms, actuator support panels, and passive transmitting diaphragms. The accelerometers were wax mounted to these surfaces and, with the exception of the actuator support panels, were positioned at their cross-sectional centers. In the case of the actuator support panels, they were mounted just outside the actuator diameters.

Up to eight Sennheiser KE 4-211-2 electret microphones (with custom amplifiers, power supplies, and housings) were used for multichannel measurements at key positions in the measurement system. The closeup view of the transmission loss measurement system in Fig. 8 shows holes drilled into the tops of the source and receiving tubes to accept relatively calibrated microphone pairs with 39.2 or 85.8 cm spacings. The upstream and downstream fields could then be decomposed following the two-microphone transfer function technique[24–26] for assessment of key partition properties within specified bandwidths and error constraints.[27] Another microphone was positioned in a hole approximately 2 cm from the source-side face of each partition to provide a reference pressure signal for automatic level adjustment of the

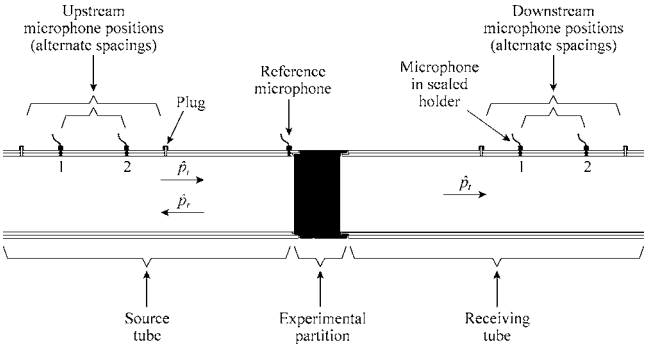

FIG. 8. A closeup view of the normal-incidence transmission loss measurement system near the arbitrary test partition. The drawing shows various microphone positions used in the measurements.

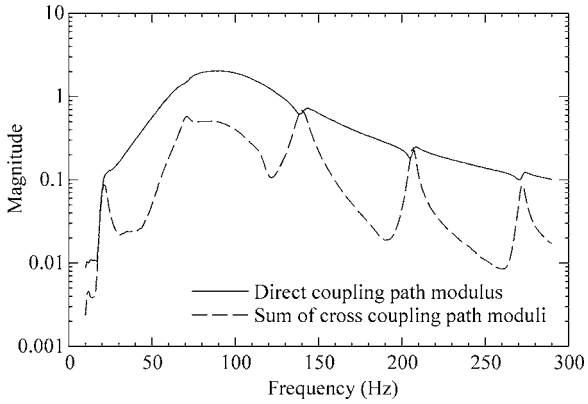

FIG. 9. The direct control path transfer function modulus and sum of cross-coupling control path transfer function moduli for one module of the DCL array.

swept sine wave stimulus used to drive the source loudspeaker.[17] As suggested in Fig. 4, four additional microphones were used to probe acoustic pressures within the cavities of the DCL ASP array. Signals derived from the microphones were used for simple monitoring purposes or to provide alternative error signals. When microphones and housings were removed from any of the holes in the system, they were replaced with airtight plugs. Brüel & Kjær model 4135 microphones (with 2633 preamplifiers and 2801 or 2803 power supplies) were also used for some measurements and as relative calibration standards for the Sennheiser microphones.

A Polytec PSV-200 scanning laser Doppler vibrometer system was used to measure transmitting normal surface vibrations of the DCL ASP. It generated operating deflection shapes[28] that increased understanding of transmitting surface behaviors. Additional details of its use are given in Sec. II F.

E. Electronics

While the electronics used in the experiments were similar to those described in Ref. 17, several of their functions were duplicated because of the increased number of controlled channels. A Hewlett-Packard 3566A PC Spectrum/Network analyzer was expanded to 16 channels. Three Krohn-Hite 3364 filter/amplifier sets (four channels each) were used instead of one. An Adcom GFA-555 power amplifier was used to drive the source loudspeaker, freeing four channels of a Luxman M-111 amplifier to drive the module actuators. Only a single dbx 1046 quad compressor/limiter was available, so it was used only to process the controller reference signal—not the four module error signals.

As indicated earlier, multiple single-error-input/single-output (MSISO) and multiple-error-input/multiple-output (MIMO) filtered-x controllers were used with the ASP arrays. Both utilized only a single reference signal derived from the signal driving the source loudspeaker amplifier. Both were implemented using a Spectrum DSP96002 system board (based on the Motorola DSP 96002 digital signal processor) and multichannel Spectrum I/O boards. While centralized multichannel controllers are commonly used in active noise control applications, a key objective of this research was to develop an ASP capable of achieving very high transmission loss over a broad bandwidth using multiple single-channel controllers. This was motivated by the expectation that individually packaged single-channel controllers could provide simplified local control for each module and thereby increase the practicality of large ASP arrays. Because the DCL ASP array was expected to produce very high transmission loss, its ability to utilize the MSISO controllers was of particular interest.

A sufficient condition for stable operation of such decentralized controllers[29] requires that the sum of cross-coupling control path transfer function moduli not exceed the direct control path transfer function modulus for any given module. Figure 9 shows these two frequency-dependent functions for one module of the array. (Because of array symmetry, plots for the other three modules were nearly identical.) The two curves reveal that the sufficient condition for stable MSISO control is met, except perhaps near 140, 206, and 272 Hz (near specific axial source tube resonance frequencies), and below about 20 Hz. In other words, the multichannel control path coupling matrix is diagonally dominant, except in these very limited spectral regions. Nevertheless, because the stated conservative condition is a sufficient but not necessary condition for guaranteed stability, the chances for successful operation across the entire bandwidth remained high.

F. Measurement capabilities and limitations

Because transducer calibration, signal derivation, signal conditioning, and postprocessing of data were conducted in manners similar to those described in Ref. 17, many of the capabilities and limitations of the experimental approach were also similar. However, several important distinctions arose in this investigation. The longer anechoic termination and wider microphone separation distances enabled lower frequency measurements. On the other hand, the square cross-sectional areas of the arrays and source and receiving tubes were much larger than those of their circular counterparts in the previous work. The highest measurement frequency was therefore much lower. Nevertheless, because the low-frequency capabilities of active partitions are of most practical interest, this limitation posed no serious problem. The more important consequence of the size and materials of the system related to an increase in flanking transmission.

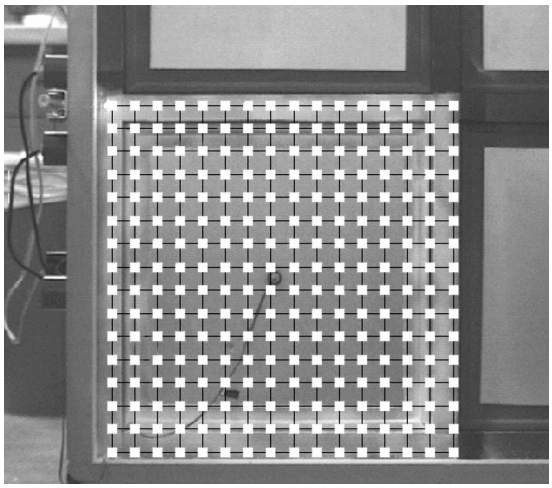

FIG. 10. Transmitting surface scan points for the scanning laser vibrometer measurement of one DCL array module.

The passive benchmark partitions discussed in Sec. II C had a variety of characteristics that helped establish the maximum bandwidth and transmission loss capabilities of the system. Through other measurements, the electroacoustic signal-to-noise ratio of the system was found to have an average value of approximately 87 dB and a minimum value no lower than 73 dB.[13] Electronic crosstalk was consistent with that discussed in Ref. 17. Neither of these concerns posed a limitation for most transmission loss measurements.

The scanning laser vibrometer measurements were only performed for the DCL ASP to verify that its transmission loss performance was in fact a by-product of efficient global control of transmitting surface vibrations. Furthermore, only a single transmitting diaphragm, its surrounding suspension, and interstice were measured as a representative sampling of the entire array. The receiving tube was removed from the measurement system to allow optical access to these transmitting surfaces. The vibrometer scanning head was positioned approximately 1.4 m away from the array. To enhance laser light detection by the head, the transmitting surfaces were coated with white (optically reflective) powder. The vibrometer system was then programmed to sequentially measure the surface vibrations at the 256 scan points indicated in Fig. 10. Using the measured results, the system generated surface plot animations representing time-harmonic structural responses (operating deflection shapes) of the surfaces. These responses were determined at different frequencies, in both passive and active states. During the measurements, the array frame was no longer sandwiched between the source and receiving tubes. It could thus vibrate against the resilient source tube gaskets with greater freedom than usual.

G. Other experimental challenges

Some of the experimental challenges discussed in Ref. 17 were again encountered with the measurements of this work. Simultaneous dynamic range requirements of the adaptive controllers and measurement systems had to be carefully addressed. Adaptive controller tracking of swept sine wave stimuli also remained a consistent challenge.

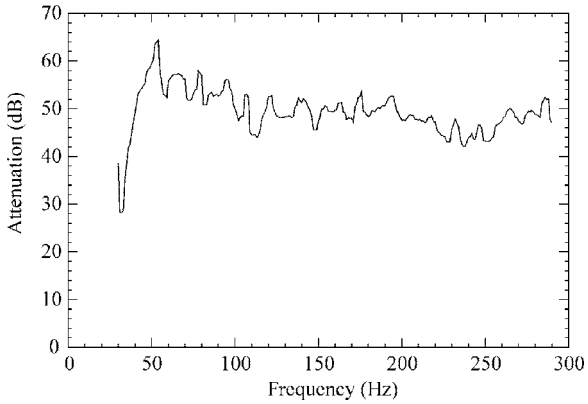

FIG. 11. The average normal acceleration error signal attenuation for the four actuator diaphragms of the SCL array.

However, flanking transmission became the matter of more serious concern as the larger experimental measurement system exacerbated its effects. Construction of sufficiently rigid and massive source and receiving tubes was difficult because of several practical constraints. Efforts were made to measure mechanical properties of their materials, fabricate rigid and massive walls, and provide resilient connections between adjacent tube sections and the floor beneath. However, the inherent structural characteristics of the large, flat tube surfaces made it difficult to minimize their vibrations sufficiently.

Another experimental challenge involved the difficulty of constraining sufficient translational piston-like motions of the ASP actuator support panels and the passive transmitting diaphragms. Even if these aluminum honeycomb sandwich panels were assumed to behave as perfect rigid bodies, nonuniformities in their spaced dual suspensions could have produced rotational components of vibration. Significant effort was expended to create suspensions that helped constrain translational motions, but both physical and fabrication limitations bounded their capabilities. Additional design effort and more precise manufacturing might have improved their behaviors.

III. RESULTS

A. Single-composite-leaf (SCL) array

The SCL array depicted in Figs. 2 and 3 was first evaluated in its passive mode, with all actuator terminals open circuited. It was subsequently evaluated when the normal accelerations of its actuator diaphragms were minimized through MSISO adaptive control (see Sec. II E). This section considers error signal reductions achieved in the latter state then presents the normal-incidence transmission losses measured in both states.

The error signal attenuations measured for each of the four modules were very similar. The average attenuation is plotted in Fig. 11 as a function of frequency. The frequency-averaged value of this curve over the controlled measurement bandwidth (30–290 Hz) was 50 dB. The steep drop to relatively poor attenuation below 50 Hz was likely caused by actuator nonlinearities below their resonance frequencies. The actuators were not effective below about 30 Hz.

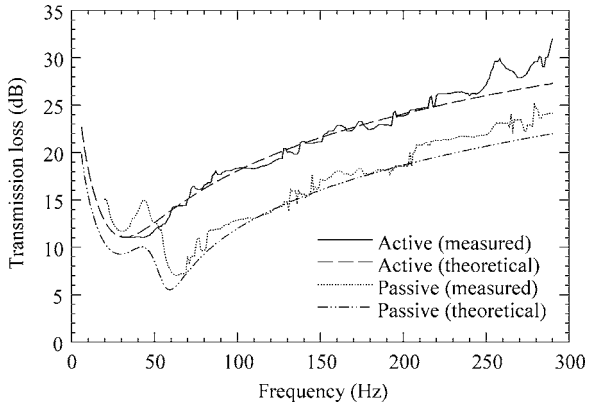

FIG. 12. Measured transmission losses for the SCL array in its active and passive states. The measured curves are plotted against theoretical predictions.

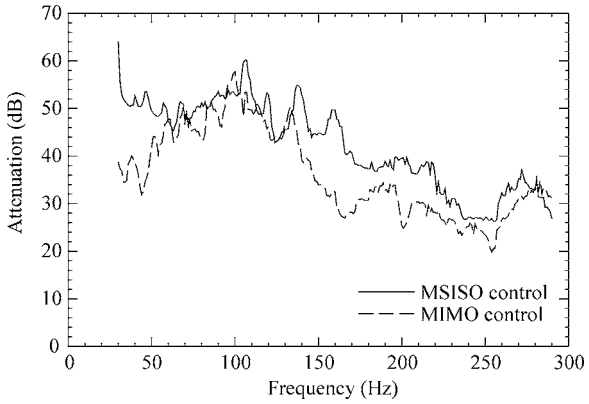

FIG. 13. Average normal acceleration error signal attenuations for the four transmitting diaphragms of the DCL array under MSISO and MIMO control.

Measured normal-incidence transmission losses of the array are plotted in Fig. 12 for both passive and active control conditions. They are also plotted against theoretical predictions based on analytical results,[16,30] as well as published, measured, and estimated parameter values.[23] In the passive mode, the array produced an average transmission loss of approximately 17 dB over the measurement bandwidth (20–290 Hz). The curve exhibits a small dip to 12 dB centered at 30 Hz and a much deeper dip to 7 dB centered at 63 Hz (near the resonance frequency of the accelerometer-loaded actuators). The array appears to be mass-controlled above 63 Hz, with a consistent rise in transmission loss of approximately 6 dB per octave. It agrees reasonably well with theoretical predictions. Once the normal accelerations of the actuator diaphragms were actively minimized, transmission loss noticeably increased over most of the measurement bandwidth. Over the controlled bandwidth, the average transmission loss was 22 dB. The resulting curve demonstrates a consistent increase of approximately 6 dB per octave at higher frequencies. It also agrees well with theoretical predictions.

B. Double-composite-leaf (DCL) array

The DCL array depicted in Figs. 4 and 5 was similarly evaluated with all actuator terminals open circuited, then with its normal transmitting diaphragm accelerations minimized through adaptive control. The control was alternately implemented using the MIMO and MSISO controllers (see Sec. II E). This section first investigates error signal reductions, controller convergences, and observed stability for the two schemes. It subsequently presents normal-incidence transmission losses for the array and compares them to those of the massive benchmark partitions and the SCL array. It then concludes with a discussion of scanning laser vibrometer measurements.

1. Error signal reduction, controller convergence, and stability

Similar error signal attenuations were again measured for each of the four modules. Average attenuations produced by the MIMO and MSISO schemes are plotted in Fig. 13 as a function of frequency. Under MIMO control, attenuations varied from 20 to 58 dB, with a frequency-averaged value of 36 dB over the controlled measurement bandwidth. Notable declines in attenuation were evident above and below 100 Hz. Attenuation under MSISO control varied from 22 to more than 60 dB, producing a frequency-averaged value of 42 dB—a full 6 dB greater than that produced by the MIMO controller. It exhibited notable improvement in attenuation below 60 Hz and between 135 and 280 Hz. In some cases, the improvement was greater than 15 dB. Outside these bandwidths, the two control schemes performed on par with one another.

It is worthwhile to consider the mechanism by which the transmitting diaphragm accelerations were minimized. As discussed in Ref. 16, the net volume velocities into the module cavities were expected to approach zero. To validate this prediction for a single module, the normal acceleration of an actuator diaphragm and that of its surrounding support panel were measured in the actively controlled state using relatively calibrated accelerometers. The volume velocities of the elements were then estimated from these measurements and the effective radiating surface areas (including pertinent surround halves). (The estimation assumed that the surfaces behaved as ideal translational pistons.) Relative levels and phases of the computed volume velocities varied slightly over frequency. However, when averaged over the controlled measurement bandwidth, the levels were within 0.7 dB and the phase difference was 162 degrees. Thus, although the agreement between the theoretical prediction and these rough experimental measurements was not exact, the primary mechanism for controlling normal transmitting diaphragm motion was basically validated.

The convergence behaviors of the two adaptive control systems were measured near source tube resonance and antiresonance frequencies for comparison. Figure 14 shows typical error signal convergences for all channels of the MIMO controller at 65 Hz (near the resonance frequency of 70 Hz). The relatively long 20 s convergence time was common near many of the source tube resonance frequencies. It is immediately evident from the plots that the convergences of all modules were in unison, as expected for the MIMO

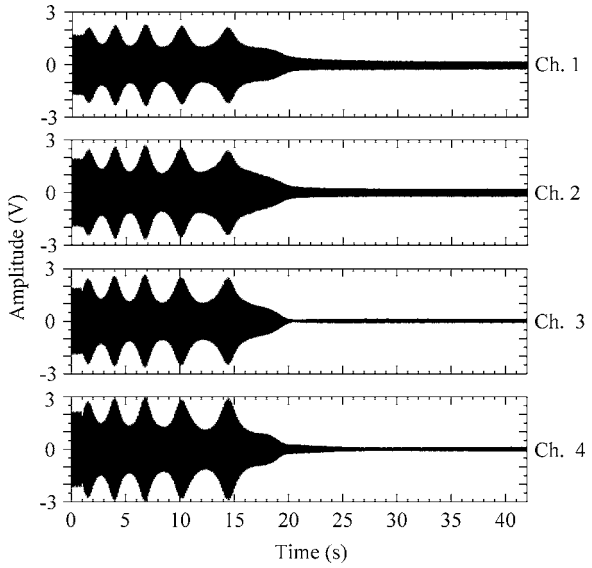

FIG. 14. Initial error signal convergences for the four channels of the MIMO controller when controlling the DCL array at 65 Hz (near the source tube resonance frequency of 70 Hz). The adaptation process begins at time approximately equal to 1 s.

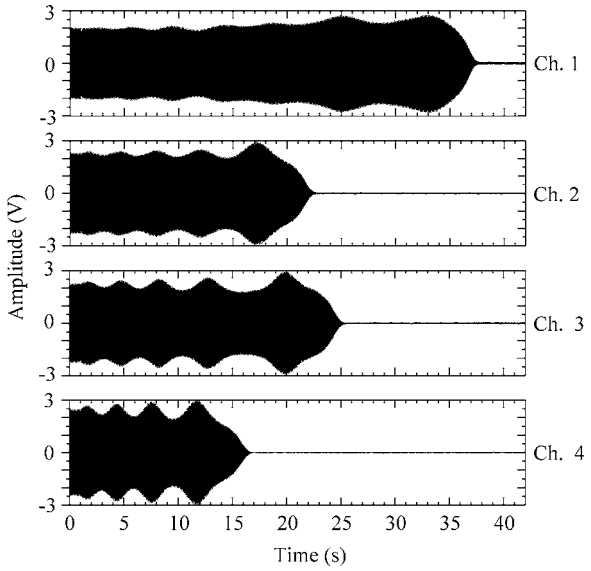

FIG. 16. Initial error signal convergences for the four SISO controllers when controlling the DCL array at 65 Hz (near the source tube resonance frequency of 70 Hz). The adaptation process begins at time approximately equal to 1 s.

controller. Several oscillatory cycles were required to reach the final steady-state condition that minimized the sum of mean-square-error values.

Figure 15 shows initial convergence plots for the MIMO controller operating at 100 Hz (near the antiresonance frequency of 105 Hz). In this case, the convergence time was only 2 s. Convergence of all channels was again simultaneous, but it proceeded with minimal oscillation and yielded notably smaller residual mean-square error values.

Initial convergence characteristics for the MSISO controllers were also investigated at these same two frequencies. Figure 16 shows typical convergence plots at 65 Hz. It is obvious from the plots that the modules did not generally converge in unison. Several oscillatory cycles were again required to reach the final steady state conditions that minimized individual mean-square-error values. The residual error signals were relatively small in comparison to those produced by the MIMO controller at this frequency. The convergence times for the various modules varied from 16 to 37 s, with an average of about 25 s. Although convergence parameters of the four SISO controllers were identical, different initial coefficient values for their passive on-line system identification algorithms may have affected individual convergence times.

The MSISO convergences at 100 Hz are shown in Fig. 17. They proceeded with few oscillatory cycles, producing

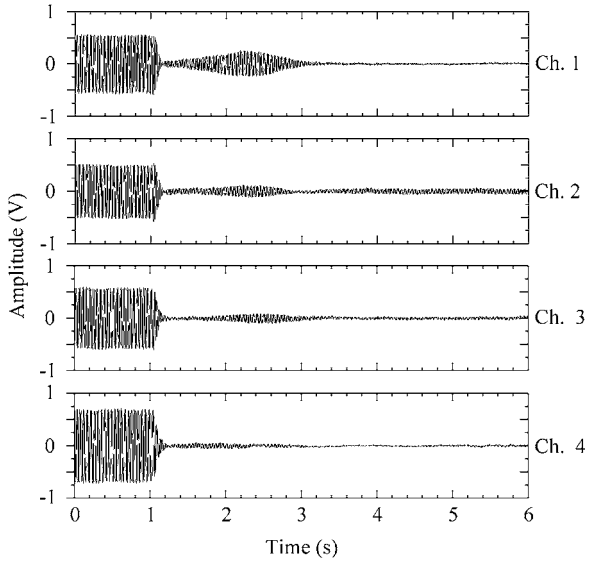

FIG. 15. Initial error signal convergences for the four channels of the MIMO controller when controlling the DCL array at 100 Hz (near the source tube antiresonance frequency of 105 Hz). The adaptation process begins at time approximately equal to 1 s.

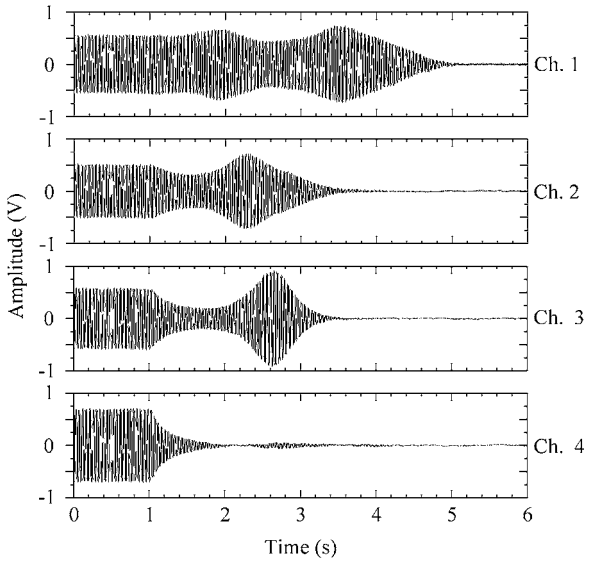

FIG. 17. Initial error signal convergences for the four SISO controllers when controlling the DCL array at 100 Hz (near the source tube antiresonance frequency of 105 Hz). The adaptation process begins at time approximately equal to 1 s.

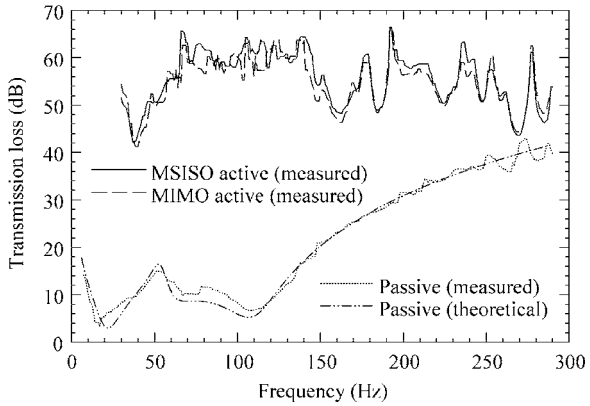

FIG. 18. Measured transmission losses for the DCL array in its active and passive states. The two active states involve either MSISO control or MIMO control. The passive transmission loss is plotted against a theoretical prediction.

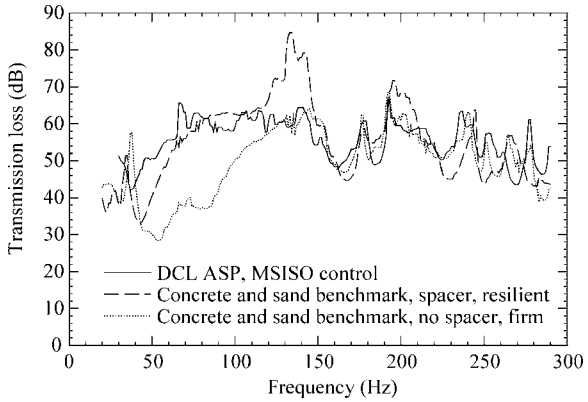

FIG. 19. Measured transmission loss for the DCL array under MSISO control. The curve is plotted against measured transmission losses for the massive double-leaf benchmark partition (concrete and sand-filled leaves) with two spacing and interconnection conditions.

convergence times between 2.5 and 4 s, and an average of about 3 s. Residual steady state error signals were again relatively small.

In addition to the convergence characteristics just considered, the stability and robustness of the controllers were matters of concern. From this standpoint, the initial convergence plots of Figs. 14–17 are somewhat misleading. Although the MIMO controller did converge well at most fixed frequencies, it had difficulty tracking the swept sine wave stimulus in certain spectral regions (e.g., near the first source tube resonance frequency of 70 Hz) with sufficient stability. In such problematic regions, the MIMO controller would often appear to converge after a long period, only to become unstable and diverge sometime later. Yet there was no indication that the control path transfer function matrix was ill conditioned for MIMO control at these or any other frequencies within the controlled measurement bandwidth.[31] It thus became necessary to adjust convergence parameters to sufficiently slow and guarantee convergence with changing stimulus frequencies. Invariably, the MSISO controllers were more stable than the MIMO controller under these same conditions. As shown earlier, their error signal attenuations were also generally superior.

The stability of the MSISO controllers was investigated under other circumstances of practical interest. The behaviors of the converged controllers were observed when control signals supplied to one or more of the array actuators were abruptly disconnected. These behaviors might be considered representative of their behaviors in applications wherein one or more ASP modules became unexpectedly disturbed. Again, these characteristics were monitored near axial resonance and antiresonance frequencies of the source tube. In every case tested, slight disturbances were noted in the other module error signals, but the controllers remained stable and quickly reconverged (i.e., in less than 1 s).

2. Normal-incidence transmission losses

Normal-incidence transmission losses of the DCL ASP are plotted in Fig. 18 for the one passive and two active conditions. The passive curve is also plotted with good agreement against a theoretical curve determined from analytical results,[16,30] as well as published, measured, and estimated module parameters.

In the passive mode, the array behaved much like a double-leaf partition. It exhibited a fundamental resonance frequency at about 17 Hz and something similar to a mass-air-mass resonance frequency at about 108 Hz. The partition appeared to be stiffness controlled below 17 Hz and produced an increase in transmission loss of slightly more than 18 dB per octave above 108 Hz. The average transmission loss over the measurement bandwidth was 22 dB.

Under MIMO transmitting diaphragm acceleration control, the average transmission loss over the controlled bandwidth (30–290 Hz) rose to 55 dB. However, the curve did exhibit several notable undulations. The minimum measured value was 41 dB, whereas the maximum measured value was 66 dB, pushing the measurement capabilities discussed in Sec. II C.

Under MSISO control, the average transmission loss over the controlled measurement bandwidth was 56 dB. This was a 33 dB improvement over that produced by the passive mode. Between 30 and 150 Hz the average improvement was 47 dB. Once again, the controlled transmission loss curve had no specific trend over frequency. In similarity to the MIMO control case, there was a prominent dip to a value of 42 dB centered at 38 Hz and other dips to values near 45 dB surrounding the source tube antiresonance frequencies of 175 and 245 Hz. The minimum measured transmission loss was 42 dB and the maximum was again 66 dB.

3. Transmission loss comparisons

To better understand the transmission loss characteristics under active control, it is worthwhile to make a few important comparisons. Because MSISO control produced slightly better performance, it alone is considered in this discussion. Measured results for the massive double-leaf benchmark partition (see Sec. II C) and the SCL array are used as standards of comparison.

The transmission loss for the active DCL array is again plotted in Fig. 19 against two measured transmission losses for the massive benchmark partition with both concrete and

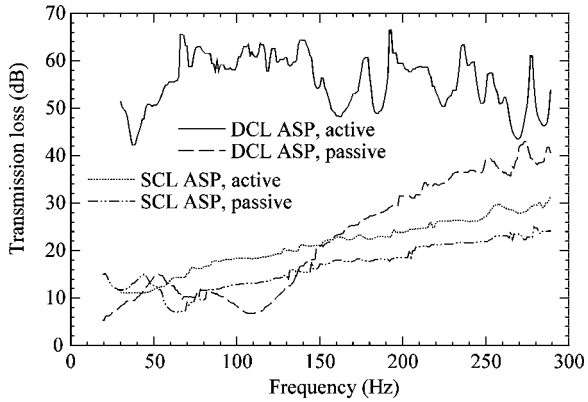

FIG. 20. Measured transmission losses for the SCL and DCL ASP arrays in their completely passive modes (actuator terminals open circuited) and under diaphragm acceleration control.

sand-filled leaves. The first benchmark measurement was made with the spacer and resilient clamping between leaves; the second was made with no spacer and firm clamping. The actively controlled array appears to perform on par with the much more massive benchmark partition in its two embodiments. (Recall from Sec. II C that transmission loss values much greater than 60 dB are considered to be uncertain.) When averaged over the controlled measurement bandwidth, the transmission loss of the array is basically equal to that of the benchmark partition involving the spacer and resilient clamping. In some spectral regions (e.g., near the benchmark low-frequency resonance dip) it performs better, but in other regions it performs worse. The ASP array produces an average 6 dB transmission loss improvement over that of the benchmark partition with small spacing and firm clamping. It performs much better than the structure between 40 and 120 Hz, the general region of its resonance dip. The array might have performed even better at the lowest control frequencies had the actuators not exhibited an increase in nonlinear behavior below 50 Hz. Limitations in controller performance may have produced other deficiencies. Based on the discussion in Sec. II C, it is also possible that flanking transmission limited the measurable transmission loss values for the array over much of the measurement bandwidth.

Additional insights follow from direct comparison of the DCL and SCL array transmission losses, as measured in their passive and active states. Figure 20 shows that the active DCL array consistently produced much higher transmission loss than the active SCL array, but its improvement was generally greater at lower frequencies than at higher frequencies. Within the controlled measurement bandwidth, the average improvement was 34 dB. The maximum improvement was 51 dB at 66 Hz and the minimum improvement was 16 dB at 269 Hz. Thus, although the objective of controlling normal principal transmitting surface vibrations was the same for both arrays, a dramatic increase in transmission loss performance was accomplished through a simple configurational change.

4. Scanning laser vibrometer measurements of transmitting surfaces

Normal vibrations of the DCL array transmitting surfaces were measured using the Polytec scanning laser vibrometer as discussed in Secs. II D and II F. Point-by-point measurements (see Fig. 10) were taken at 100 and 200 Hz in the passive state and in the active state produced by MSISO control.

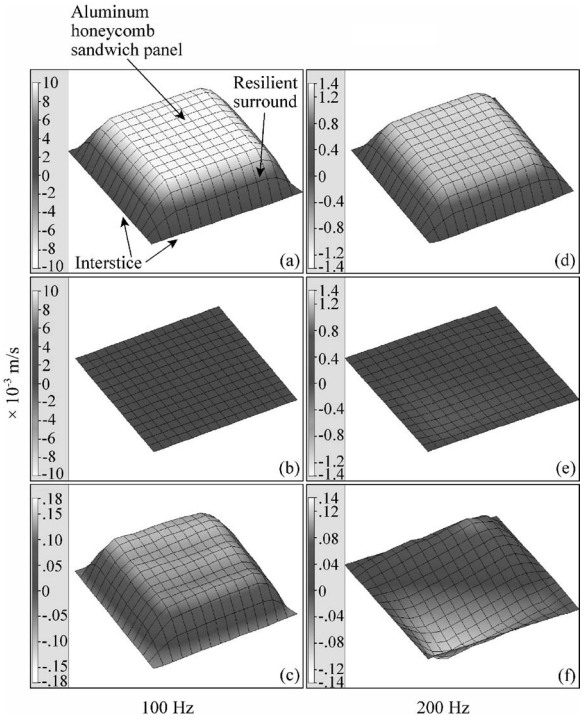

FIG. 21. Operating deflection shape images for the transmitting surfaces of an individual DCL ASP module. (a) Passive mode, 100 Hz. (b) Normal transmitting diaphragm acceleration control, 100 Hz. (c) Normal transmitting diaphragm acceleration control, magnified scale, 100 Hz. (d) Passive mode, 200 Hz. (e) Normal transmitting diaphragm acceleration control, 200 Hz. (f) Normal transmitting diaphragm acceleration control, magnified scale, 200 Hz.

Figure 21(a) shows an operating deflection shape visualization of the transmitting diaphragm, resilient suspension, and interstice for a single passive module with 100 Hz excitation. Figure 21(d) shows a similar result for 200 Hz excitation. Animations of the shapes showed that the transmitting diaphragm (central portion of each image) behaved as a nearly ideal translational piston at both frequencies. Though not apparent from Fig. 21(d), there was a slight "wobble" detectable in the response at 200 Hz, but it was almost insignificant. The resilient surround appeared to flex consistently around the periphery of the piston at both frequencies. Interstice vibration, represented by the outermost points of the images, was undetectable in the 100 Hz animation, and was only slightly detectable in the 200 Hz animation.

When normal acceleration at the center of the transmitting diaphragm was actively minimized, the surfaces exhibited the responses shown in Figs. 21(b) and 21(e) at 100 and 200 Hz, respectively. From these images, it is clear that normal vibration was efficiently and globally minimized at both frequencies—fulfilling a key design objective. Fine details of the minute residual vibrations were difficult to ascertain with the same amplitude scales used for the passive mode. The scales were consequently adjusted to magnify the responses as shown in Figs. 21(c) and 21(f). These images reveal several interesting characteristics.

At 100 Hz, the maximum normal vibration was reduced by approximately 37 dB. Judging from the 53 dB normal acceleration attenuation shown for this frequency in Fig. 13, it is evident that the reduction did not represent the maximum that might have been achieved. There are a few reasons for this. First, the vibrometer measurements were intended chiefly to demonstrate spatial responses of the vibrating surfaces under passive and active conditions. The same attention to signal gain structures and control optimization was therefore not considered as important for these measurements. Because the normal acceleration of the panel was reduced to nearly the threshold of the centrally mounted accelerometer, the accelerometer could not reliably provide signal for further attenuation. Initial excitation levels (seen in the passive state) might have been increased or an accelerometer with a lower threshold might have been employed to demonstrate greater vibration attenuation capabilities. In addition, control filter coefficients were adapted *a priori* for this case, then held constant over the duration of the vibrometer scans to enable reasonably time-invariant conditions for the point-by-point measurements. Without the typical continuous adaptation of control filter coefficients (which might have produced ambiguous operating deflection shapes), a less-than-maximal error signal attenuation resulted.[32]

It is apparent from Fig. 21(c) that the residual transmitting diaphragm vibration at 100 Hz continued to be piston-like in nature. A small amount of rippling is evident over the diaphragm area that may have been an artifact of measurement noise. The surround also continued to flex in a consistent manner around the diaphragm at all measurement points. A small in-phase residual interstice vibration was apparent from the animations at the magnified scale. As suggested earlier, such motion should be expected—even for a perfectly stiff frame—because the array was mounted resiliently to the source tube, and was not sandwiched between it and the receiving tube. Despite the motion, the small cross-sectional area of the interstice would have produced inefficient radiation into a receiving space.

The 200 Hz residual response shown in Fig. 21(f) reveals a more interesting vibrational pattern. The maximum normal vibration (near the opposing deflected corners) was reduced by approximately 21 dB relative to the passive piston-like amplitude. Once again, this attenuation might be contrasted with the 40 dB normal acceleration attenuation found in Fig. 13 at the same frequency for the center point of the transmitting diaphragm. Figure 21(f) shows this point to have more significantly reduced motion than many other positions. Animations also clarified that the residual vibration consisted of a rocking motion about a nearly diagonal line. The motion appeared to be a combination of the two rotational rigid-body modes about the centered Cartesian axes parallel to the module edges.

Fortunately, this dipole-like motion is known to produce very inefficient radiation into a receiving space. In the case of the plane-wave receiving tube, a surface dipole with zero volume velocity would produce zero radiation to downstream positions. In a three-dimensional receiving space, its radiation would be finite but very small if the dimensions of the diaphragm were small compared to wavelength. At 200 Hz, the dimensions certainly met this requirement. Furthermore, when several adjacent modules demonstrate this type of vibrational behavior, the overall multipole order of the ASP can become much higher than a dipole, producing even less efficient radiation.[33]

Additional vibrometer measurements verified that the tendency of the transmitting diaphragm to exhibit residual rotational rigid-body motion was greater at higher frequencies than at lower frequencies. The field behind the diaphragm became less and less uniform with increasing frequency and would therefore tend to excite the diaphragm with a less symmetric pressure distribution. However, it is likely that this residual rocking motion could have been reduced through improved manufacturing processes. Any nonuniformities or imbalances in the diaphragm suspensions or fin structures might have induced the problem—even with a uniform pressure distribution behind the diaphragm.

IV. SUMMARY AND CONCLUSIONS

Experimental methods have been developed to measure normal-incidence transmission losses of two lightweight active segmented partitions (ASPs) in their passive and active states. The first ASP consisted of four single-composite-leaf (SCL) modules with lightweight moving-coil actuators mounted within resiliently suspended support panels. The second consisted of four double-composite-leaf (DCL) modules that used the first array to electroacoustically actuate isolated cavities that were bounded on the opposite sides by passive transmitting diaphragms. The control objective for each array was to globally reduce normal transmitting surface vibrations through the simple actuation and sensing of principal transmitting surfaces, and to consequently produce high transmission loss.

The DCL ASP used this vibration control scheme much more efficiently than the SCL ASP. It also satisfied several other design and performance criteria established earlier. Its high transmission loss capabilities could not be completely evaluated because of flanking transmission limitations in the measurement system. Nevertheless, its average transmission loss over the measurement bandwidth was determined to be 56 dB—a full 34 dB greater than that of the SCL ASP. In addition, its average value was 47 dB higher in the typically challenging low-frequency range between 30 and 150 Hz. These substantial increases resulted from a simple configurational change in the array—not from considerable changes in underlying control objectives or system complexities.

The measured passive and active transmission losses agreed well with theoretical estimates, suggesting that previously developed models had useful predictive capabilities. Other measurements verified that a predicted zero source-side volume velocity condition for the DCL modules was principally responsible for controlling their normal transmitting diaphragm vibrations.

The DCL ASP was successfully controlled using multiple-error-input, multiple-output (MIMO) and multiple single-error-input/single-output (MSISO) filtered-x controllers. The decentralized MSISO controllers produced an aver-

age error signal attenuation (in transmitting diaphragm acceleration) that was approximately 6 dB greater than that produced by the centralized MIMO controller. Although average convergence times were slightly longer for the decentralized controllers, they remained very stable when one or more of the array actuators were abruptly disturbed. They were also more stable than the MIMO controller near source tube resonance frequencies. These results demonstrate that the ASP was amenable to independent single-channel controllers—a matter of importance for practical implementations.

Scanning laser vibrometer measurements of the DCL ASP verified that its high transmission loss was produced primarily by efficient global reductions in its normal transmitting surface vibrations. Although minute residual vibrations were detectable in its controlled state, they were either so small in amplitude or produced such inefficient transmission into the receiving space that they were of minor importance.

This work has shown that lightweight ASPs can be practically and locally controlled to produce very high transmission loss at lower audible frequencies, far exceeding transmission losses of passive partitions with comparable masses. When properly configured, they can achieve this result through global reduction of normal transmitting surface vibrations. While this work and previous work have demonstrated promising results for DCL configurations, they have also increased awareness of issues requiring further investigation. Transmission losses of ASPs should be carefully investigated using oblique and random-incidence fields. Sound transmission should be analyzed in near fields and far fields of three-dimensional receiving spaces. The impact of vibrating interstices and their flexural responses should also be studied. Alternative types of actuators and controllers should be developed and work should be conducted to further decrease overall ASP masses and thicknesses. Bidirectional capabilities of ASPs (i.e., their abilities to produce active sound transmission control in either direction between adjacent acoustic spaces) should also be studied and developed. The authors encourage research in these and other areas to enhance the viability of ASPs as sound transmission control tools.

ACKNOWLEDGMENTS

The authors gratefully acknowledge financial and other support for portions of this project from the Penn State University Graduate Program in Acoustics. They also acknowledge the Penn State Applied Research Laboratory, Rapid Die and Molding Company, Hewlett-Packard Company, Young-Cheol Park, Scott Sommerfeldt, Karl Reichard, and Courtney Burroughs for their contributions and input to the project. They finally thank Joye, Lara, Lane, and Rachel Leishman for meaningful assistance in the assembly of the transmission loss measurement system.

[1]J. E. Cole, III and M. C. Junger, "Active noise control for machinery enclosures," NSF Final Report U-1944-379F, 1991.
[2]D. R. Thomas, P. A. Nelson, and S. J. Elliott, "An experimental investigation into the active control of sound transmission through stiff light composite panels," Noise Control Eng. J. **41**, 273–279 (1993).
[3]D. R. Thomas, P. A. Nelson, R. J. Pinnington, and S. J. Elliott, "An analytical investigation of the active control of the transmission of sound through plates," J. Sound Vib. **181**, 515–539 (1995).
[4]S. L. Sharp, G. H. Koopmann, and W. Chen, "Transmission loss characteristics of an active trim panel," Proceedings of Noise-Con 97, University Park, PA, 1997, Vol. **2**, pp. 149–160.
[5]M. E. Johnson and S. J. Elliott, "Active control of sound radiation from vibrating surfaces using arrays of discrete actuators," J. Sound Vib. **207**, 743–759 (1997).
[6]R. L. St. Pierre, Jr., G. H. Koopmann, and W. Chen, "Volume velocity control of sound transmission through composite panels," J. Sound Vib. **210**, 441–460 (1998).
[7]J. E. Cole, K. F. Martini, and A. W. Stokes, "Active noise control for machinery enclosures," NSF Final Report U-2413-393, 1996.
[8]S. M. Hirsch, J. Q. Sun, and M. R. Jolly, "An analytical study of interior noise control using segmented panels," J. Sound Vib. **231**, 1007–1021 (2000).
[9]S. M. Hirsch, N. E. Meyer, M. A. Westervelt, P. King, F. J. Li, M. V. Petrova, and J. Q. Sun, "Experimental study of smart segmented trim panels for aircraft interior noise," J. Sound Vib. **231**, 1023–1027 (2000).
[10]T. W. Leishman and J. Tichy, "A fundamental investigation of the active control of sound transmission through segmented partition elements," Proceedings of Noise-Con 97, University Park, PA, 1997, Vol. **2**, pp. 137–148.
[11]T. W. Leishman and J. Tichy, "An experimental evaluation of individual partition segment configurations for the active control of sound transmission," J. Acoust. Soc. Am. **104**, 1776(A) (1998).
[12]T. W. Leishman and J. Tichy, "An experimental investigation of a novel active segmented partition for sound transmission control," J. Acoust. Soc. Am. **105**, 1156(A) (1999).
[13]T. W. Leishman, "Active control of sound transmission through partitions composed of discretely controlled modules," Ph.D. thesis, The Pennsylvania State University, University Park, PA, 2000.
[14]T. W. Leishman, "Vibration-controlled modules for use in active segmented partitions," J. Acoust. Soc. Am. **114**, 2385(A) (2003).
[15]T. W. Leishman, "Research in the field of active sound transmission control," J. Acoust. Soc. Am. **114**, 2390(A) (2003).
[16]T. W. Leishman and J. Tichy, "A theoretical and numerical analysis of vibration-controlled modules for use in active segmented partitions," J. Acoust. Soc. Am. **118**, 1424–1438 (2005).
[17]T. W. Leishman and J. Tichy, "An experimental investigation of two module configurations for use in active segmented partitions," J. Acoust. Soc. Am. **118**, 1439–1451 (2005).
[18]Previously established criteria for effective ASPs have suggested that adjacent modules should have sufficiently weak cross-coupling control paths to facilitate use of decentralized single-channel adaptive controllers.
[19]Additional details concerning the measurement system and procedures are found in Refs. 13 and 17.
[20]P. E. Doak, "Excitation, transmission and radiation of sound from source distributions in hard-walled ducts of finite length. I. The effects of duct cross-section geometry and source distribution space-time pattern," J. Sound Vib. **31**, 1–72 (1973).
[21]Slight transmission loss measurement errors were caused by the nonanechoic condition below 45 Hz.
[22]Arithmetic decibel averages are used in this paper.
[23]B. E. Anderson and T. W. Leishman, "An acoustical measurement method for the derivation of loudspeaker parameters," AES 115th Convention, New York, 2003, Preprint 5865, pp. 1–13.
[24]J. Y. Chung and D. A. Blaser, "Transfer function method of measuring in-duct acoustic properties. I. Theory," J. Acoust. Soc. Am. **68**, 907–913 (1980).
[25]J. Y. Chung and D. A. Blaser, "Transfer function method of measuring in-duct acoustic properties. II. Experiment," J. Acoust. Soc. Am. **68**, 914–921 (1980).
[26]"Standard test method for impedance and absorption of acoustical materials using a tube, two microphones, and a digital frequency analysis system," American Society for Testing and Materials, ASTM Designation: E 1050-90, 1990.
[27]H. Bodén and M. Åbom, "Influence of errors on the two-microphone method for measuring acoustic properties in ducts," J. Acoust. Soc. Am. **79**, 541–549 (1986).
[28]M. H. Richardson, "Is it a mode shape, or an operating deflection shape?," Sound Vib. **31**, 54–61 (1997).

[29]S. J. Elliott and C. C. Boucher, "Interaction between multiple feedforward active control systems," IEEE Trans. Speech Audio Process. **2**, 521–530 (1994).
[30]The analytical predictions of Ref. 16 were adapted to account for the small surface areas of the rigid MDF interstices.
[31]P. A. Nelson and S. J. Elliott, *Active Control of Sound* (Academic, London, 1992).
[32]One might assume a one-to-one correspondence between transmitting surface vibration attenuation and transmission loss increase. However, transmission loss is a function of both transmitted and incident sound power. The latter cannot always be considered constant. The introduction of active sound transmission control changes the terminating boundary condition of the source tube and therefore changes the source tube field, including the incident sound power.
[33]I. L. Vér and C. L. Holmer, "Interaction of sound waves with solid structures," in *Noise and Vibration Control*, revised ed., edited by L. L. Beranek (Institute of Noise Control Engineering, Washington, DC, 1988), Chap. 11.